Depressed myocardial cross-bridge cycling kinetics in a female guinea pig model of diastolic heart failure

Sukriti Dewan, Namthip Witayavanitkul, Mohit Kumar, Beth Mayer, Lauren Betancourt, Olivier Cazorla, Pieter de Tombe

Depressed myocardial cross-bridge cycling kinetics in a female guinea pig model of diastolic heart failure

Sukriti Dewan1,2□, Namthip Witayavanitkul1,2□, Mohit Kumar2□, Beth J. Mayer2□, Lauren Betancourt3□, Olivier Cazorla3□, and Pieter P. de Tombe1,2,3□

.....
.....
1 Department of Physiology and Biophysics, College of Medicine, University of Illinois at Chicago, Chicago, IL, USA;

2 Department of Cell and Molecular Physiology, Stritch School of Medicine, Loyola University Chicago, Maywood, IL, USA;

3 Phymedexp INSERM, CNRS, University of Montpellier, Montpellier, France.

Correspondence to Pieter P. de Tombe: pdetombe@uic.edu

Cardiac hypertrophy is associated with diastolic heart failure (DHF), a syndrome in which systolic function is preserved but cardiac filling dynamics are depressed. The molecular mechanisms underlying DHF and the potential role of altered cross-bridge cycling are poorly understood. Accordingly, chronic pressure overload was induced by surgically banding the thoracic ascending aorta (AOB) in ~400 g female Dunkin Hartley guinea pigs (AOB); Sham-operated age-matched animals served as controls. Guinea pigs were chosen to avoid the confounding impacts of altered myosin heavy chain (MHC) isoform expression seen in other small rodent models. In vivo cardiac function was assessed by echocardiography; cardiac hypertrophy was confirmed by morphometric analysis. AOB resulted in left ventricle (LV) hypertrophy and compromised diastolic function with normal systolic function. Biochemical analysis revealed exclusive expression of β-MHC isoform in both sham control and AOB LVs. Myofilament function was assessed in skinned multicellular preparations, skinned single myocyte fragments, and single myofibrils prepared from frozen (liquid N2) LVs. The rates of force-dependent ATP consumption (tension-cost) and force redevelopment (Ktr), as well as myofibril relaxation time (Timelin) were significantly blunted in AOB, indicating reduced crossbridge cycling kinetics. Maximum Ca2+ activated force development was significantly reduced in AOB myocytes, while no change in myofilament Ca2+ sensitivity was observed. Our results indicate blunted cross-bridge cycle in a β-MHC small animal DHF model. Reduced cross-bridge cycling kinetics may contribute, at least in part, to the development of DHF in larger mammals, including humans.

Introduction

Heart failure (HF), a syndrome in which the heart is unable to meet the body's demands for cardiac output, is linked to poor clinical outcomes (Pfeffer et al., 2019; Tsao et al., 2022). Diastolic heart failure (DHF) or HF with preserved ejection fraction (HFpEF) is a clinical syndrome reported in >50% of HF cases, wherein the systolic function of the heart is preserved but cardiac filling dynamics are depressed (Maeder and Kaye, 2009). Population-based studies indicate that DHF is more common in hypertensive elderly females than in males (Maeder and Kaye, 2009). In contrast, most animal models of HF studied to date have been performed in male subjects, of which even fewer animal models have been developed to study DHF. At the cellular level, HF has been associated with imbalanced ion-channel gating, disturbed calcium homeostasis, and depressed myofilament function in both human and experimental animal models (Bers, 2002; van der Velden and de Tombe, 2014; van der Velden and Stienen, 2019). The precise molecular mechanisms underlying depressed myofilament function in HF, and in particular the diastolic dysfunction form of the syndrome remain largely unknown.

Actomyosin cross-bridge cycling kinetics underly the mechanical performance of the heart. Myosin's enzymatic activity is the biochemical basis of cross-bridge chemo-mechanical coupling, a process whereby ATP is hydrolyzed to generate energy to fuel muscle force production and muscle shortening under mechanical load (Gordon et al., 2000; de Tombe, 2003; van der Velden and Stienen, 2019). Actomyosin ATPase activity and muscle shortening velocity are tightly coupled to the MHC isoform (de Tombe and ter Keurs, 2012). α-MHC is the faster molecular motor, displaying three- to fivefold faster actinactivated ATPase activity, time to peak systole, shortening velocity, and cross-bridge cycling kinetics compared with β-MHC (van der Velden et al., 1998; Rundell et al., 2005; Locher et al., 2009; Chen et al., 2010; Locher et al., 2011; de Tombe and ter Keurs, 2012). Most of the studies documenting depressed crossbridge cycling kinetics in the failing heart have been done either in rats or

mice (Rundell et al., 2004; Daniels et al., 2007; Zobel et al., 2007; Patel et al., 2017). Rats and mice almost exclusively express the alpha isoform of myosin (α-MHC) in their ventricles. A pertinent confounding result is that small rodents exhibit a metabolic switch toward the β-MHC isoform under higher workload or pathological conditions (Rundell et al., 2004; Rundell et al., 2005; Belin et al., 2007; Daniels et al., 2007). This phenomenon confounds the interpretation of these studies because the shift in MHC isoform expression likely dominates the reduced cross-bridge dynamics observed in rats and mice under pathophysiological conditions, thus masking the potential role of cross-bridge cycling dynamics in human HF (Daniels et al., 2007). The impacts of such an isoform switch are largely absent in failing human hearts as ~95% expression levels of β-MHC isoformare observed in healthy human myocardium (de Tombe, 1998; Hasenfuss, 1998; Miyata et al., 2000; Riehle and Bauersachs, 2019; Pilz et al., 2022). Data from failing human hearts have shown depressed cross-bridge cycling kinetics (van der Velden, 2011). Though very useful, human studies are difficult to interpret due to many uncontrolled factors in obtaining tissue samples and the lack of adequate controls (Hasenfuss, 1998; Marston and de Tombe, 2008). Nonetheless, evidence is emerging that altered myofilament kinetics may play a contributive role toward the development of HF.

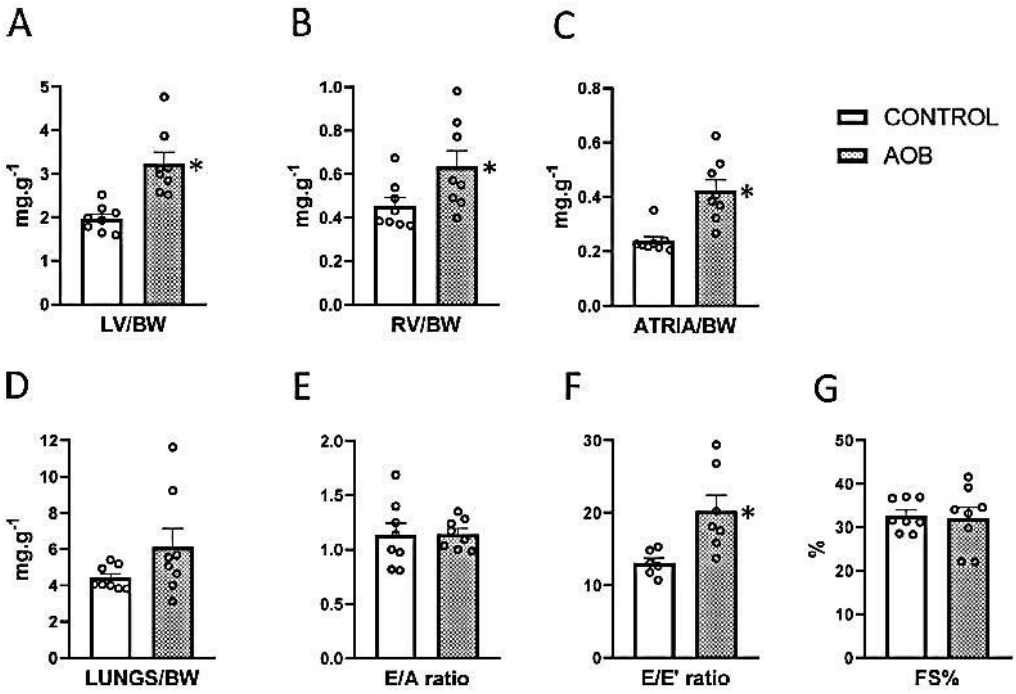

Figure 1. In vivo signs of hypertrophy and diastolic heart failure in AOB. 16 wk following AOB (n = 8 hearts), signs of cardiac hypertrophy were evident from increases in the weights of the LV (A; P = 0.0006), right ventricle (B; P = 0.045), and atria (left and right auricles combined; C; P = 0.0009). Pulmonary congestion was evident from a trending increase in lung wet weight (D; P = 0.124). All weights were normalized to body weight and expressed as mg/gram. Diastolic LV dysfunction was evidenced by a pseudo-normalized E/A ration (E; P = 0.94) with an increase in the Doppler echocardiography E/E9 ratio (F; P = 0.014). In contrast, echocardiography-derived fractional shortening was not affected by AOB (G; P = 0.83). Sham-operated animals (n = 8 hearts) served as controls. Additional echocardiography data are presented in Fig. 2. Sham control, open bars; AOB, closed bars. *P = 0.05 by unpaired t test.

Guinea pigs predominantly express the β-MHC isoform in their ventricles, even in juvenile states (Malhotra et al., 1992; van der Velden et al., 1998). Few groups have studied the guinea

pig model of pressure-overload HF induced by aortic banding (AOB; Lecarpentier et al., 1987; Siri et al., 1989; Johns et al., 1999). However, most of those studies focused on either steady-state conditions or membrane-intact isolated cardiac muscle preparations. To gain a clearer understanding of crossbridge cycling kinetics in DHF, we developed a hypertensive guinea pig model in a β-MHC background by AOB in female animals. Non-invasive echocardiography confirmed the development of cardiac hypertrophy and diastolic dysfunction, suggesting the presence of HFpEF. Skinned myocardium isolated from the hearts of these animals revealed altered myofilament function that included prolonged myofibril relaxation time, depressed maximum force development, reduced tension cost, and blunted rate of force redevelopment. These results show blunted cross-bridge cycle kinetics in a small animal HF model in the absence of any alterations in myosin isoform composition. Reduced cross-bridge cycling kinetics may be an important contributor to the development of DHF in larger mammals, including humans.

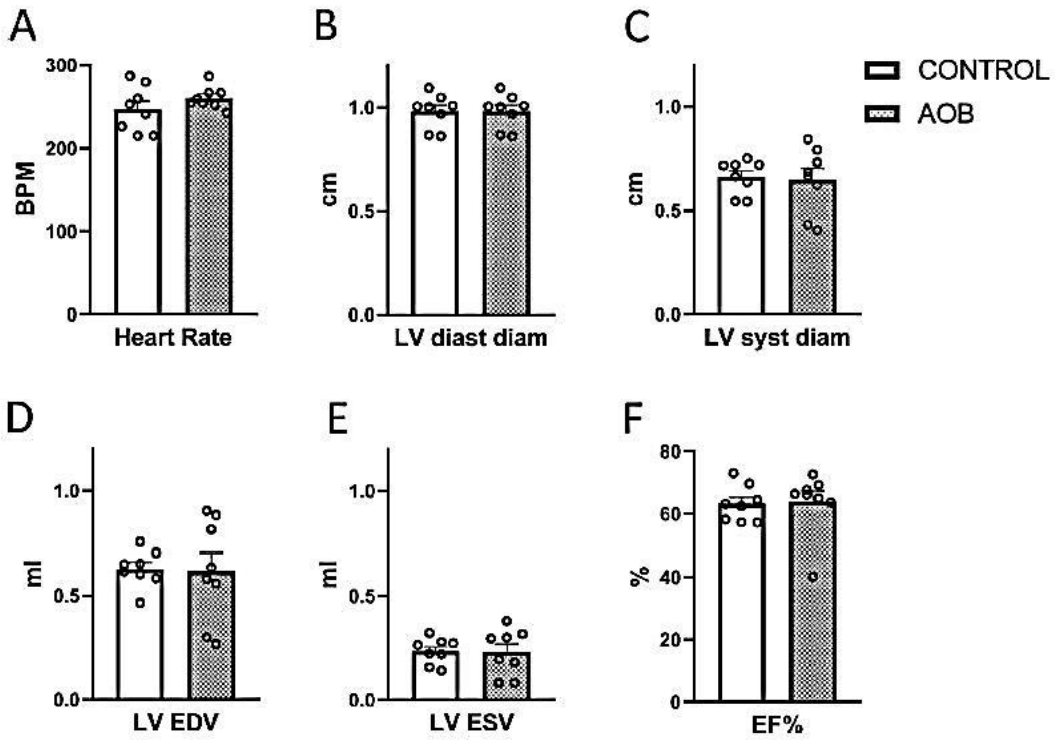

Figure 2. Additional echocardiography results. Animals were examined by 2-D and M mode echocardiography. Open bars illustrate Sham-operated and hatched bars illustrate AOB animals. Echocardiography was performed under light anesthesia (0.5% isoflurane via nose cone). Eight animals were examined in each group. (A) Heart rate in beats per minute (BPM) as recorded during the echocardiography session ($P = 0.245$). (B and C) LV diastolic (B; $P = 0.99$) and systolic (C; $P = 0.90$) diameter derived from 2-D echocardiography. (D and E) LV volumes were estimated by assuming a spherical LV to calculate end-diastolic (D; LV EDV; $P = 0.99$) and end-systolic (E; LV ESV; $P = 0.82$) volume. Estimated LV volumes were used to calculate the estimated LV ejection fraction: EF% = (EDV − ESV)/EDV (F; $P = 0.87$). There were no significant differences between the Sham and AOB group for these parameters.

Materials and methods

Animal model

All animals were treated and housed in accordance with the Animal Care and Use Committee guidelines at the University of Illinois at Chicago Biologic Resources Laboratory. Mechanical pressure overload was induced in guinea pigs (n = 8 animals) as described previously (Lecarpentier et al., 1987; Siri et al., 1989; Malhotra et al., 1992; Wang et al., 1999b; Foster et al., 2016). Briefly, female Dunkin Hartley guinea pigs weighing ~400 g were intubated by tracheotomy and maintained on isoflurane anesthesia (2%) using positive pressure ventilation for the entire surgical procedure. Following thoracotomy, the thoracic ascending aorta was surgically banded using 3-0 monofilament polypropylene suture around an 18-gauge needle resulting in ~50% aortic stenosis. A further, additional, group of sham operated age-matched animals (n = 8 animals) served as controls. Animals were allowed to recover in a heated cage before being returned to the animal facility and monitored during the next 16 wk to both observe and document the physical wellbeing of the animals; analgesia was administered as required, mostly within the first 2 wk after surgery. In a small cohort of animals, just prior to sacrifice under deep anesthesia (see below), measurements of peak LV systolic and diastolic pressures revealed an approximately twofold increase in both pressures in AOB animals.

At the end of the study period, serial M-mode and 2-D echocardiography were performed to assess cardiac architecture and function while lightly sedated using 0.5% isoflurane administered via a nose cone (Henein and Lindqvist, 2020). The next day, animals were deeply anesthetized (5% isoflurane via nose cone) and euthanized by removal of the heart and exsanguination. Immediately after the beating heart was excised from the chest, it was perfused with ice-cold phosphate-buffered saline (PBS) and weighed for its chamber masses. Portions of the tissues were snap-frozen and stored in liquid N2 (vapor phase) for all subsequent subcellular and proteomic studies. Another portion of the perfused LV was processed for tissue histology. Briefly, a cross-sectional cut of PBS-perfused LV was obtained from a region superior to the apex. The tissue slice was then immersed in a cold 10% formaldehyde solution and stored at 4°C for 1 wk. Next, the tissue was embedded in paraffin wax and sectioned with a microtome. Sections were stained to assess fibrosis (HE and Masson's trichrome) and imaged at 10× magnification under a bright field microscope equipped with a CCD camera. The area captured for imaging and analysis was kept uniform across the sections. The amount of collagen present in the LV was additionally determined using the hydroxy-proline collagen assay (Stegemann and Stalder, 1967).

Echocardiography

Serial M-mode and 2-D echocardiography were performed to assess both cardiac function and chamber dimensions (Siemens Acuson Echocardiography machine, 15 MHz pediatric probe). Derived volume measurements were based on the assumption that guinea pigs' hearts are spherical. Using the pulsed wave Doppler (PWD) and tissue Doppler imaging (TDI) capabilities, we also assessed aortic, pulmonary, mitral flow velocities, and mitral tissue movement velocities to derive E/A and E/E9 measurements to index diastolic function. All measurements were performed in lightly sedated animals (0.5% isoflurane). Animals were administered atropine (0.1 mg/kg IV) to compensate for mild depressed cardiac function due to anesthesia.

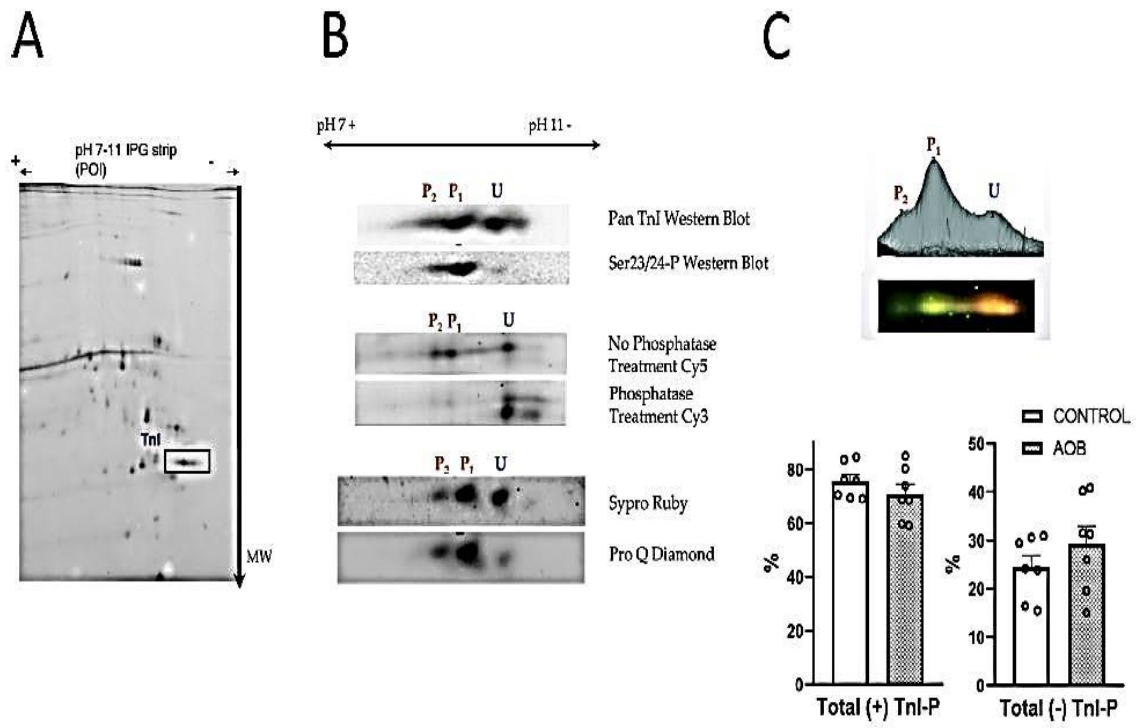

Figure 3. 2-D–DIGE analysis of TnI phosphorylation. Cardiac samples of Sham and AOB were analyzed by 2-D–DIGE. The first dimension was performed by electro focusing on IPTG strips pH range 7–11. The next dimension was performed on SDS-PAGE gels for molecular weight separation. A shows a representative 2-D–DIGE gel (pH 7–11) wherein Sham and AOB samples were tagged with Cy3 and Cy5 dyes. The TnI spots are indicated by the square box in the bottom right area of the 2-D gel. B illustrates strategies employed to identify the TnI gel spots of this sample. Top: Pan-total TnI antibody and Ser23/24 phospho-specific antibody Western blots. Middle: 2-D–DIGE analysis of untreated pooled samples stained with Cy5 and PP1, and PP2A-treated pooled samples stained with Cy3. Bottom: Sypro Ruby total protein and ProQ Diamond gel stains that identify phosphorylated proteins. From these results, we were able to identify the TnI gel spots as unphosphorylated (U), single (P1), and double phosphorylated (P2) as indicated. C shows an example of the 2-D–DIGE results where Sham and AOB differentially labeled samples are run together and analyzed by the GE Decyder 2-D–DIGE analysis package. The top panel illustrates the differential analysis based on simultaneous scanning of the Cy3 and Cy5 channels. The bottom bar graphs show the average (n = 7 for Sham and n = 7 AOB) level of unphosphorylated (U spot) and total phosphorylated (P1 + P2) cardiac TnI. On average, the phosphorylation level of TnI was slightly, albeit not significantly, decreased in the AOB group. Sham control, open bars; AOB, closed bars. Sham control vs. AOB: (+) TnI-P P = 0.299; (−) TnI-P P = 0.668). Source data are available for this figure: Source Data F3

Proteomics

Cardiac α- and β-MHC isoforms were electrophoretically separated on 1.5-mm thick, 14-cm wide, and 16-cm long gels with a Hoefer SE 600 system(Hoefer Scientific) as previously described (Rundell et al., 2005). Standard Western blotting procedures were used to confirm MHC isoforms. 1-Dmini format GE Tris-bis 4–12% SDS-PAGE gradient gels were used to separate both high and low molecular weight myofilament proteins using MOPS buffer. Staining was done using Sypro Ruby total protein stain using manufacturers' guidelines.

Myofilament phosphoproteins

2-D gel electrophoresis (Fig. 3 A) was done to separate extracted myofilament proteins based on charge and mass (Warren et al., 2008). All images generated from the DIGE experiments

were analyzed with the DeCyder software package from GE Healthcare. Phosphatase treatment, with PP1 and PP2A, of pooled samples was done on freshly homogenized samples. The samples were then labeled with Cy3 and run with non-phosphatase treated samples from the exact same pool labeled with Cy5. Image analysis was done using DeCyder. Corresponding identification of phosphorylated spots was carried out by staining gels with Pro Q diamond Stain, as per manufacturer's instructions, compared with gels that were stained with Sypro Ruby protein stain for total protein staining. In addition, Western blotting with site-specific phospho-antibodies was performed to identify phospho-specific sites within the phospho-specific spots.

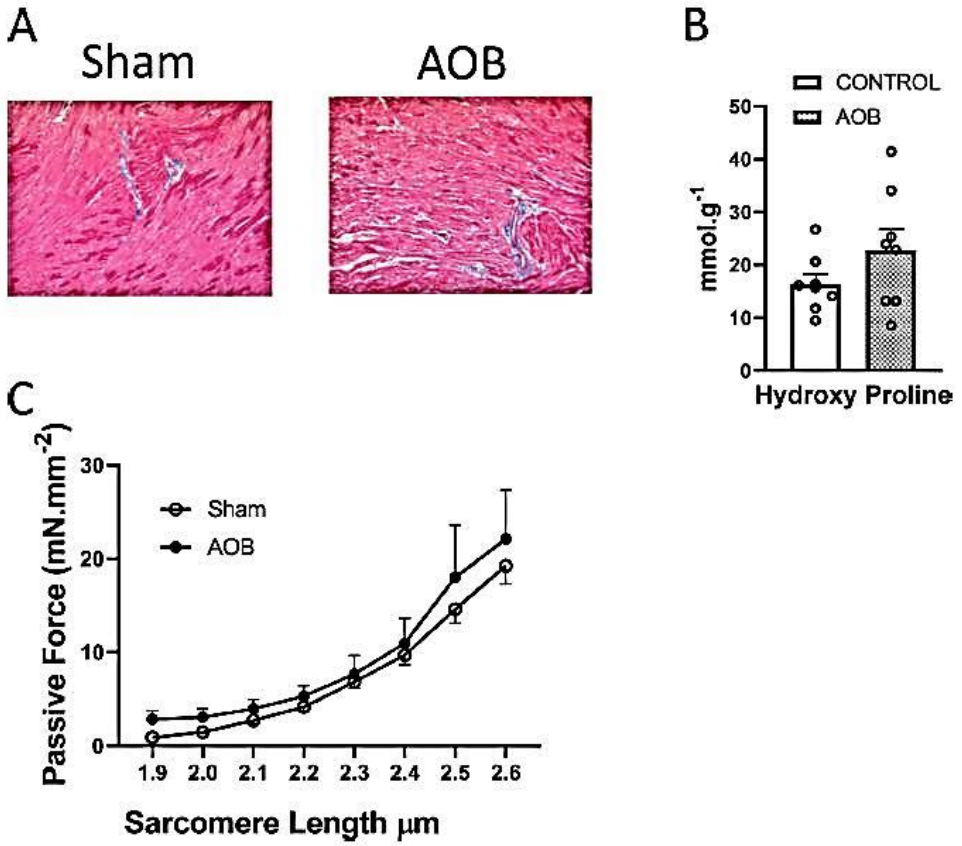

Figure 4. Fibrosis and myofilament stiffness in AOB. Formaldehyde-fixed (10%) LV tissue samples were paraffin-embedded, sectioned by microtome, and stained with HE Masson's tri-chrome. A shows representative 10× bright field images from the Sham and AOB group. A minor increase in collagen deposition is evident in AOB. The results of the more quantitative hydroxyproline collagen assessment displayed in B revealed a small, but nonsignificant, increase in collagen content in AOB (P = 0.161). Single isolated myofibrils were examined over a range of SL and no difference in myofilament passive stiffness was evident in response to AOB. Sham (n = 8 hearts; open bar) and AOB (n = 8 hearts; closed bar).

Single skinned myocytes

Myocytes (fragments) were harvested from the frozen LV tissue by mechanical homogenization (Belin et al., 2007; Ait-Mou et al., 2016). Briefly, a portion of the LV (30–40 mg) was homogenized at 10,000 rpm for 1 s in a relaxing solution (pH = 7.1) on ice. The relaxing solution contained (in mM) 97.92 KOH, 6.24 ATP, 10 EGTA, 10 Na2CrP, 47.58 K-propionate, 100 BES, 6.54 MgCl2, 1 DTT, 0.01 Leupeptin, 0.1 PMSF, and 0.001 Pepstatin (pH = 7.0). Next, the homogenate slurry was filtered through a 70-µm cell strainer, followed by centrifugation at 120 g for 1 min at 4°C. The cells were permeabilized (skinned) by resuspending the pellet in a relaxing solution with ultrapure 1% Triton-X100 (Thermo Fisher

Scientific) added for 10–15 min on a slowly rotating shaker. Thereafter, the Triton was removed by resuspending the single cells two times in a relaxing solution after centrifugation at 120 g for 1 min at 4°C. After the final centrifugation, resultant myocytes were suspended in 1 ml cold relaxing solution and kept on ice until use (up to 8 h). Permeabilized (skinned) myocytes in the relaxing solution were placed in a 0.1% BSA-coated 35-mm culture dish on the stage of an inverted microscope (Leica DMIRB). Myocytes to be studied were selected based on a visual scan at 10× magnification, identifying the uniformity of the cell and a regular striation pattern. Next, myocytes were attached to two metal microneedles connected to a Piezo translator (ThorLabs) and a force transducer (Aurora Scientific) and attached to XYZ stage manipulators. The cell attachment was accomplished using UV-sensitive glue (Norland 63). All measurements were made under bright field conditions at 40× magnification using a long working distance objective lens. The attached skinned myocyte was perfused at room temperature (about 21°C) with skinned fiber solutions emanating from a closely placed perfusion pipette attached to a solenoid valve-controlled perfusion system (VC-8M eight-channel mini-valve perfusion system, Warner Instruments). A maximum Ca2+ saturating activation solution was applied at the beginning of the experiment to test the strength of the cell attachment. Subsequently, cells were continuously perfused with relaxing solution, interspersed with random Ca2+ activating solutions with varying calcium concentrations (pCa 10.0 to pCa 4.5) to elicit an isometric force response. Sarcomere length (SL) was continuously monitored and maintained at 2.2 μm using custom-designed video microscopy–based FFT method as previously described (Fan et al., 1997). The isometric force was recorded at each activating cycle; zero baseline force level was subtracted from all force recordings. All force measurements were corrected for a rundown and normalized to the cross-sectional area. Cell cross-sectional area was measured at the end of the experiment by slackening the attached myocyte until buckling; the dimensions of the "ellipse" of the two sides of the buckled cell were measured with a calibrated TV screen monitor. Cells were discarded if their total rundown was >20%. Approximately six cells per heart were used for experiments. Subsequently, multiple individual myocyte fragment-derived data were averaged to obtain a single average datum per heart.

Simultaneous measurement of isometric force and ATPase activity

Permeabilized multicellular preparations were prepared from LV tissue by mechanical homogenization as previously described (Witayavanitkul et al., 2014). Briefly, the tissue was rapidly cut into 2–4 mm pieces (<0.04 g) in an ice-cold relaxing solution (composition as for skinned myocytes above), followed by homogenizing at low speed (600 rpm, 15 s; Power Gen 700D; Thermo Fisher Scientific) in a relaxing solution. The preparation was allowed to settle and the supernatant discarded after which the tissue was resuspended in the relaxing solution. The tissue was then permeabilized overnight with 1% Triton at 4°C, which served to remove cell membranes and intracellular membrane bound structures. The tissues were then extensively washed in fresh ice-cold relaxing solution and stored on ice and used within 8 h. The strips of muscle were selected for appearance under a dissecting microscope. They were then attached to a force transducer (KG4A; World Precision Instruments) and high-speed length controller (model 315C; Aurora Scientific) using aluminum T-Clips. Muscle dimensions were determined using an ocular micrometer mounted in the dissection microscope (resolution ~10 μm). SL was measured in the passive relaxed condition by laser diffraction and adjusted to 2.2 μm. Isometric tension and ATPase activity were measured at various levels of Ca2+ activation at 25°C as previously described (de Tombe and Stienen, 2007; Witayavanitkul et al., 2014). Briefly, the isolated muscle was exposed to a range of calcium solutions obtained by proportional mixing of activating and relaxing solutions, and

force development and ATP consumption were measured simultaneously during the contraction. Activating solution contained (in mM) 10 Ca2+-EGTA, 5.77 Na2ATPH2, 1.55 potassium propionate, 6.59 MgCl2, 100 BES, 5 sodiumazide, 1 DTT, 10 phosphoenolpyruvate, 0.01 oligomycin, 0.1 PMSF, and 0.02 A2P5, as well as protease inhibitor cocktail. The relaxing solution was identical, except it contained (in mM) 5.70 Na2ATPH2, 21.2 potassium propionate, and 7.11MgCl2. The pre-activating solution contained (inmM) 0.5 EGTA, 9.5 HDTA, 5.70 Na2ATPH2, and 21.8 potassium propionate. All solutions contained 0.5 mg/ml pyruvate kinase and 0.05 mg/ml lactate dehydrogenase (Sigma-Aldrich) and had a calculated ionic strength of 180 mM, 5 mM free MgATP, and 1 mMfree Mg2+, pH = 7.1.

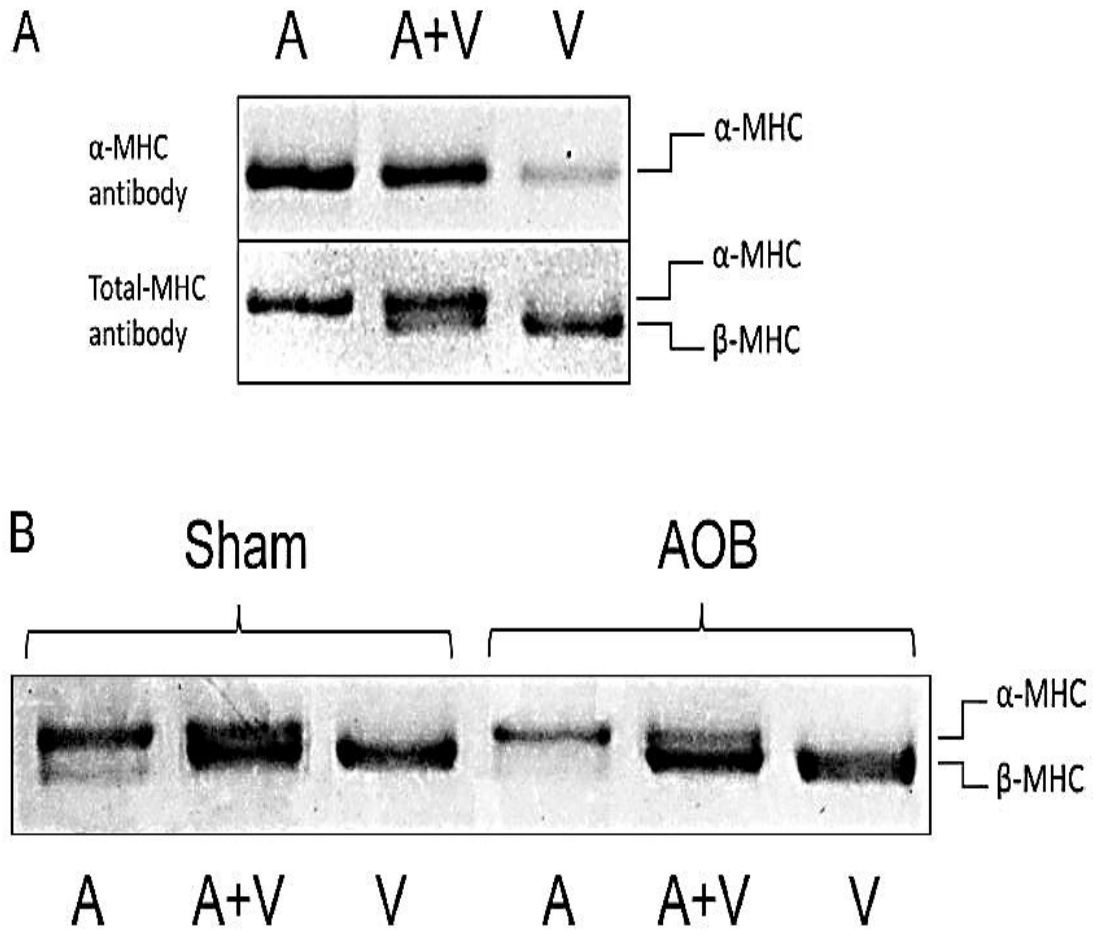

Figure 5. Cardiac MHC isoform composition. Cardiac MHC isoform composition was assessed by SDS-PAGE electrophoresis (Rundell et al., 2005). (A) Identification of protein bands by Western blot antibody staining. The three lanes shown were loaded with an atrial extract (left lane A; contains mostly α-MHC), a ventricular extract (right lane V; contains mostly β-MHC), and an atrial + ventricular mixture (middle lane A + V). An α-MHC specific antibody (top) only detected bands in the left A and middle A + V lane, while a pan-MHC (total MHC) antibody detected bands in all lanes; here, separation between the two MHC isoforms is evident. (B) Sypro Ruby total protein stain was used to measure MHC composition. Representative lanes of atrial (A), ventricular (V), and A + V are shown for a Sham and AOB cardiac sample. In all samples studied, α-MHC was below the detection limit (n = 3 Sham hearts and n = 3 AOB hearts). Source data are available for this figure: Source Data F5

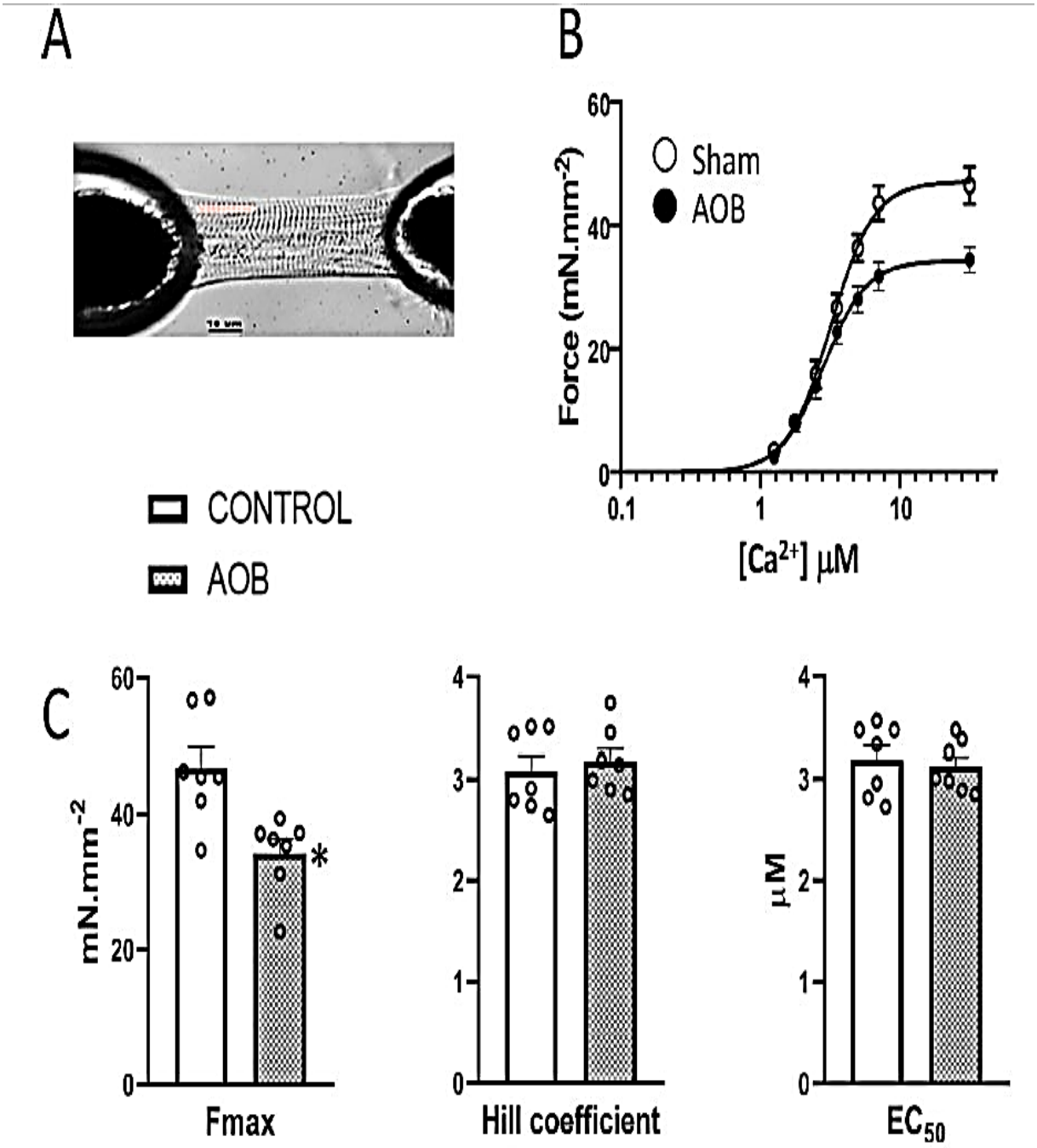

Figure 6. Skinned myocyte Ca2+ activated force development. (A) Representative skinned isolated myocyte fragment mounted in the experimental chamber using optical glue (SL = 2.2 µm; room temperature; 10 µm calibration bar). (B) Average force–[Ca2+] relationships in Sham and AOB. (C) Average Hill parameters obtained in the Sham (open bars) and AOB (closed bars) groups. Force was normalized to cross-sectional area (Sham n = 7 hearts; AOB n = 7 hearts). Approximately six myocytes were studied per heart. Subsequently, multiple muscle data were averaged to derive a single average datum per heart. *P = 0.05 (Fmax P = 0.005; Hill parameter P = 0.614; EC50 P = 0.664).

The muscle ATPase activity was measured by a UV-coupled optical absorbance enzyme assay (van der Velden et al., 1998; de Tombe and Stienen, 2007; Witayavanitkul et al., 2014). Briefly, ATP hydrolysis into ADP and inorganic phosphate inside the skinned muscle was coupled to the oxidation of NADH to NAD+, catalyzed by pyruvate kinase and lactate dehydrogenase at 25°C. Since NADH absorbs light at 340 nm and NAD+ does not, the oxidation of NADH to NAD+, and thus ATP consumption, was determined by measuring the

absorbance of UV light at 340 nm at steady state within the measurement chamber. This absorbance signal was calibrated by repeated injections of 50 nl of 10 mM ADP into the measuring chamber. The ADP injection induced a rapid-step reduction in absorbance, and the rate of ATP consumption was calculated by the magnitude of this step from the absorbance decay rate at 340 nm. In addition, the ADP injection served to confirm that the chemical response time and bath stirring were adequate. Furthermore, the rate of force redevelopment following a release–restretch maneuver (Ktr) was measured during a final contraction at maximum Ca2+. Only muscles that maintained >80% maximal tension were included for analysis. Approximately three muscles were studied per heart. Subsequently, multiple individual muscle-derived data were averaged to obtain a single average datum per heart.

Single myofibrils

Single myofibrils experiments followed previously described procedures (Poggesi et al., 2005; Stehle et al., 2009; Vitale et al., 2021). Briefly, myofibrils were prepared by high-speed homogenizing skinned surgically cut tissue strips isolated from frozen LV-free wall tissue (18,000 rpm for 9 s). Single myofibril experiments were performed using a custom-built perfusion bath that was mounted on the stage of an inverted microscope (Olympus IX-70; 40× bright field). Myofibrils were attached to two glass needles (∼30 and ∼7 µm, respectively). The smaller needle was bent 90° to form a cantilever. This was used to measure myofibril force by means of split photodiode calibrated position detection on the magnified image of the cantilever projecting from the microscope front camera port. Force was normalized to the cross-sectional area. An attached myofibril was subjected to three contraction–relaxation cycles by rapid solution switching to either pCa 4.0 or pCa5.7 (resting SL = 2.2 µm; 15°C); force data were averaged for these three contraction cycles. The passive force–SL relationship was recorded for each myofibril under still bath conditions in the relaxing solution at 15°C by stretch from SL = 1.9 to 2.6 µm in 0.1 µm increments. Up to 30 myofibrils were studied per experimental cohort (CON or AOB). Subsequently, multiple individual myofibril-derived data were averaged to obtain a single average datum per heart.

Data analysis and statistics

Statistical measures of significant differences either employed Student's t test or two-way ANOVA (GraphPad Prism). A P value < 0.05 was considered significant.

Results

Guinea pig DHF model

4mo of moderate to severe aortic stenosis (AOB; ∼50%) resulted in significant increases in LV (Fig. 1 A), right ventricular (Fig. 1 B), and atrial (Fig. 1 C) weights, indicating cardiac hypertrophy. Furthermore, an increase in the lung wet weight was observed in the AOB group (Fig. 1 D), indicative of pulmonary congestion. In addition, LV contraction relaxation was impaired in the AOB group as evidenced by the significant increase in the E/E9 parameter (Fig. 1 F). This echocardiography parameter is a sensitive measurement of cardiac relaxation dynamics; a marked increase in this metric is the hallmark of diastolic dysfunction (Henein and Lindqvist, 2020). However, the E/A ratio was not impacted by AOB (Fig. 1 E). These observations are consistent with clinical indices of restrictive cardiomyopathy with blunted relaxation and DHF, wherein a pseudo-normalized E/A ratio has been documented (Zile and Brutsaert, 2002). In contrast, LV contractility was not altered in AOB, as indexed by the

fractional shortening parameter (Fig. 1 G). This echocardiography-derived parameter is equivalent to the LV ejection fraction of the heart as a pump. Overall, these observations in the AOB group are consistent with the syndrome of congestive heart failure. Moreover, these data are also consistent with DHF and HFpEF (Pfeffer et al., 2019). Additional echocardiography data are presented in Fig. 2.

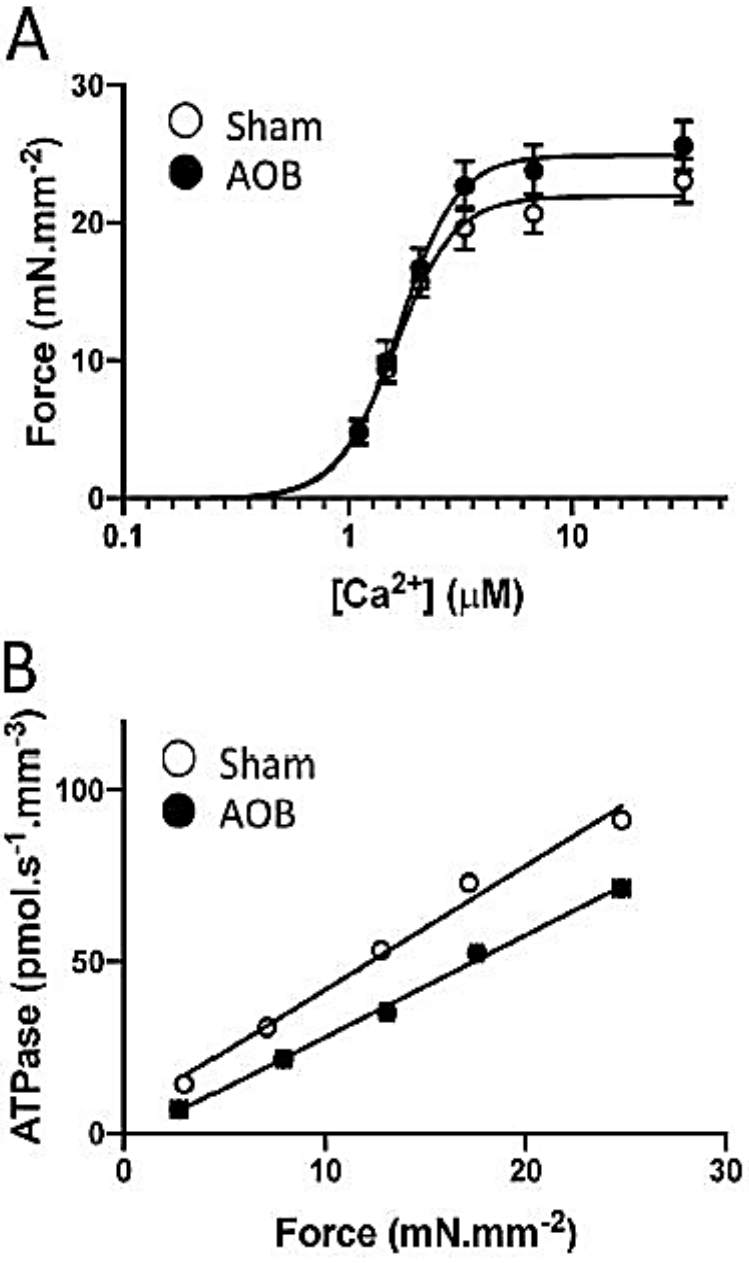

Figure 7. Isometric force and ATPase activity. Multicellular trabecula-like skinned muscle preparations were isolated from frozen samples by mechanical dissociation (Witayavanitkul et al., 2014). Force and simultaneous ATPase activity were measured by an enzyme-coupled assay (n = 8 hearts per group; approximately three preparations/heart; SL = 2.2 μm; 25°C). (A) Average force–[Ca2+] relationship in Sham (open symbols) and AOB (closed symbols) groups. (B) Average force–ATPase activity relationship in Sham and AOB multicellular preparations. Force is normalized to cross-sectional area and ATPase activity is normalized to muscle volume (length times cross-sectional area). The slope of this relationship is termed tension-cost, the magnitude of force dependent cross-bridge ATP consumption rate, which is inversely proportional to cross-bridge detachment rate. Approximately three muscles were studied per heart. Subsequently, multiple muscle data were averaged to derive a single average datum per heart.

Myofilament phosphoproteins

Analysis of the changes in phosphoprotein levels was done by the 2-D DIGE technique. The first dimension of the 2-D gels was run in the ranges of pH 3–11 for myosin binding protein C (MyBP-C); pH 4–7 for tropomyosin (Tm), troponin T (TnT), myosin light chain 1 and 2 (MLC-1 and MLC-2); and pH 7–11 for troponin I (TnI; Fig. 3). The second dimension was run on 12% SDS-PAGE gels on a large format to obtain maximum resolution. No significant changes were found in the phosphoprotein profiles of MyBP-C, Tm, MLC-2 and MLC-1, or TnT between the Sham or AOB group. Three spots or density peaks (U, P1, P2) were identified for TnI by Western blotting of pH 7–11 2-D gels (Fig. 3 B, top panel). Upon phosphatase treatment with PP1 and PP2A, only one spot remained for TnI (spot U), confirming the other two spots to be phosphorylation modifications (P1, P2; Fig. 3 B, middle panel). Finally, ProQ diamond staining of the pH 7–11 2-D gels (Fig. 3 B, bottom panel) further confirmed that spots P1 and P2 for TnI were phosphorylated modifications. Thus, two spots (P1, P2) corresponded to phosphorylation sites and one spot on the right (U) corresponded to the unphosphorylated sites in guinea pig TnI. A small, albeit nonsignificant, decrease was found in the phosphoprotein levels of TnI in the AOB group (Fig. 3 C).

Fibrosis and passive stiffness

Ventricular hypertrophy-associated fibrosis may contribute to restricted cardiomyopathy by increasing myocardial stiffness, thereby impeding ventricular filling. However, qualitative histological analysis of fixed LV tissue samples revealed only minor increases in collagen disposition in the AOB group (Fig. 4 A). This finding was further confirmed by a more quantitative measurement, the hydroxy-proline assay, which showed a modest albeit nonsignificant increase in collagen in the AOB group (Fig. 4 B). Another source of myocardial stiffness may derive from the cardiac myofilaments themselves. Measurement of passive force in single myofibrils over a range of SLs revealed no differences between Sham or AOB single myofibrils (Fig. 4 C).

Hence, the DHF syndrome observed in the AOB group is unlikely to result from passive mechanical restrictions to LV filling.

Myosin isoform composition

Small rodents, unlike humans, express predominantly the fast isoform of the myosin heavy chain (α-MHC), which is replaced by β-MHC expression under conditions of cardiac stress. Guinea pigs are reportedly an exception to this rule. To confirm this important experimental parameter, we subjected cardiac tissue samples from Sham and AOB hearts to electrophoretic analysis using methods we have previously developed (Rundell et al., 2005). Separation of guinea pig MHC isoforms, notoriously difficult, was indeed accomplished as demonstrated by Western blot isoform identification using both a specific (human) α-MHC antibody (Fig. 5 A, top) and a pan-MHC antibody (Fig. 5 A, bottom). Of note, the α-MHC containing atrium was used as a positive control. Gel separation and total protein quantification (Fig. 5 B) revealed a close to 100% LV β-MHC composition in both Sham and AOB hearts.

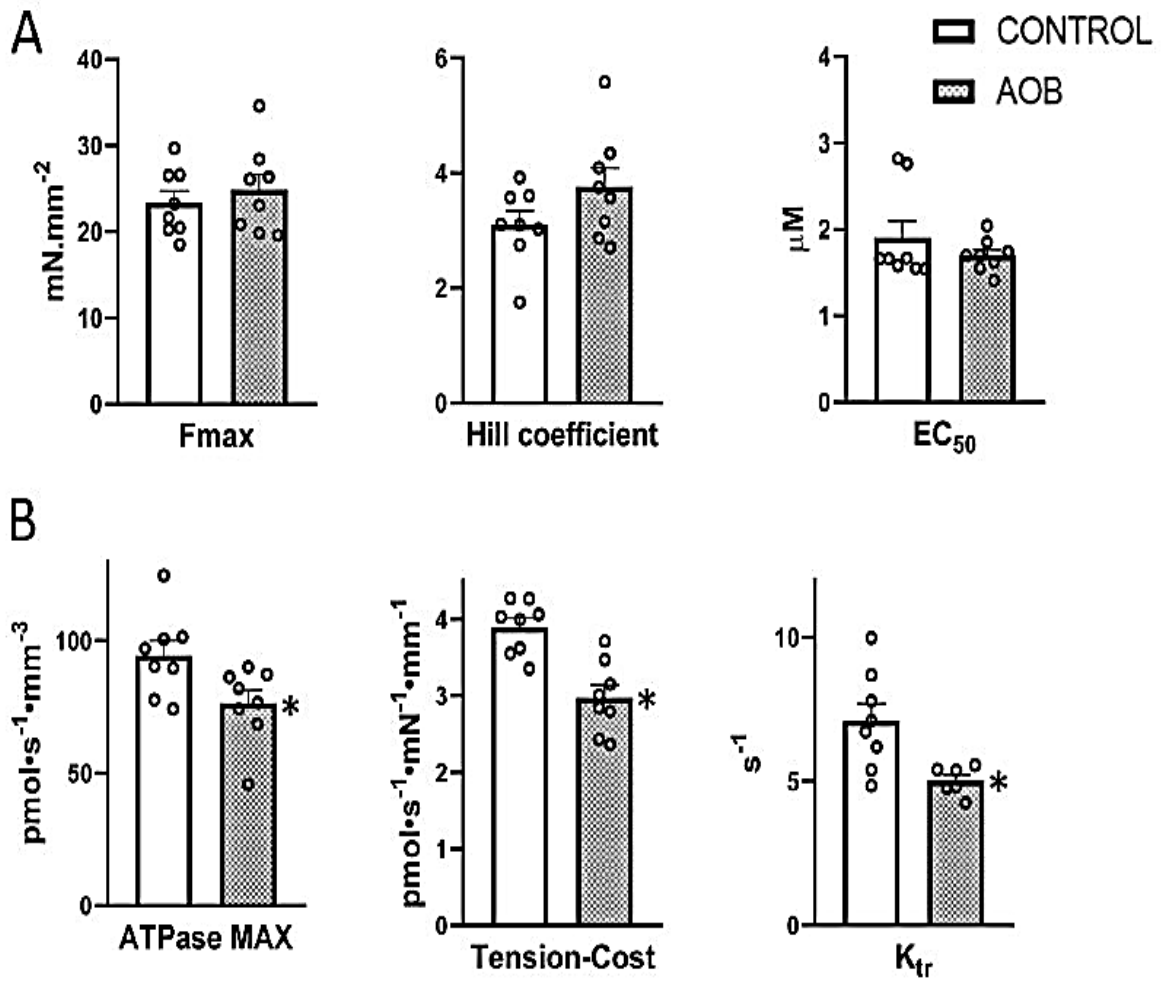

Figure 8. Force–Ca2+ responsiveness, tension-cost, and Ktr in skinned multi-cellular preparations. (A) Average Hill fit parameters of Ca2+ dependent force in Sham (open bars) and AOB (closed bars). (B) Average maximum ATPase consumption rate, tension-cost, and Ktr, the rate of force redevelopment following a rapid release–restretch maneuver, (n = 8 hearts per group; 25°C). Approximately three muscles were studied per heart. Subsequently, multiple muscle data were averaged to derive a single average datum per heart. *P = 0.05. Individual P vales: Fmax: P = 0.522; EC50: P = 0.338; Hill parameter: P = 0.128; ATPase max: P = 0.023; tension-cost: P = 0.005; Ktr: P = 0.015.

Skinned myocyte Ca2+ responsiveness

To gain insight into the impact of AOB on myofilament function, isometric force development of skinned myocyte fragments isolated from frozen LV free wall (Fig. 6 A)were assessed over a range of activating [Ca2+] at SL = 2.2 µm. The average force–[Ca2+] relationship is displayed in Fig. 6 B, while the average Hill fit parameters derived from each individual myocyte fragment are shown in Fig. 6 C. Neither myofilament Ca2+ responsiveness nor the Hill coefficient (slope) was affected by AOB. In contrast, the maximum Ca2+ saturated force was significantly reduced in the AOB group. The decrease in isometric maximal tension in single skinned myocytes suggests that the sarcomeres are dysfunctional in DHF despite the preserved systolic function of the cardiac pump. This suggests that sarcomeric dysfunction is an intrinsic phenotype of DHF.

Tension-cost

Dynamic isometric myofilament properties were assessed by measurement of force-dependent ATP consumption rate (tension-cost) in multi-cellular skinned preparations over a range of activating [Ca2+] at 25°C and SL = 2.2 μm. In addition, at the end of the tension-cost protocol, a fast release–restretch maneuver was employed to measure the Ktr parameter. Fig. 7 A shows the average force–[Ca2+] relationship obtained in the Sham and AOB groups, while Fig. 7 B shows typical examples of the relationship between ATPase activity and force development in a Sham and AOB muscle. The slope of this relationship is termed tension cost and is theoretically proportional to 1/g, the inverse of the cross-bridge detachment rate (Brenner, 1991). Average-derived parameters for the Sham and AOB groups are presented in Fig. 8.

There was no significant difference in the force–[Ca2+] relationship between the Sham and the AOB groups. In contrast, the overall ATP consumption rate as well as the force-dependent ATPase rate (tension-cost) were significantly reduced in the AOB group, indicating a reduction in cross-bridge cycling rate. This finding is consistent with the significant reduction in Ktr seen in the AOB group, a parameter that also indexes crossbridge cycling rate.

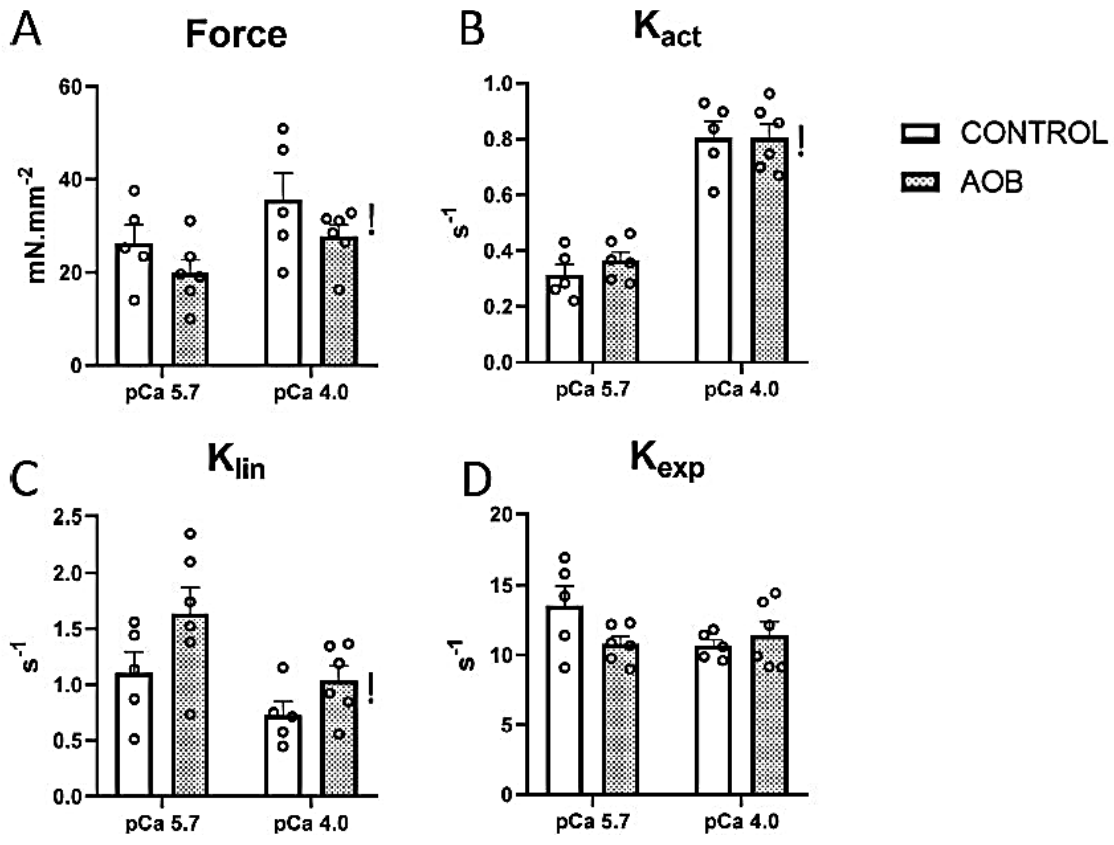

Figure 9. Additional single myofibril parameter results. Single myofibrils were isolated from the hearts of sham control (open bars) and AOB (closed bars), mounted in the experimental apparatus by two glass probes, and subsequently underwent Ca2+ activation/relaxation cycles by means of a rapid solution change. Myofibrils were activated either at ~50% maximum (pCa = 5.7), or at saturating Ca2+ (pCa = 4.0). n = 5 hearts per group, up to 30 myofibrils were studied per cohort, SL 2.2 μm, 15°C. Subsequently, multiple muscle data were averaged to derive a single average datum per heart. Data were analyzed by twoway ANOVA. (A) Steady-state myofibril force development (Force): P = 0.035 Ca2+ impact, P = 0.075 AOB impact. (B) Ca2+ activation kinetics (Kact): P = 0.0001 Ca2+ effect, P = 0.553 AOB impact. (C) Linear relaxation rate (Klin), P = 0.003 Ca2+ impact, P =

0.110 AOB impact. (D) Exponential relaxation rate (Kexp),P = 0.241 Ca2+ impact, P = 0.304 AOB impact). !, P = 0.05 pCa 4.0 vs. pCa 5.7.

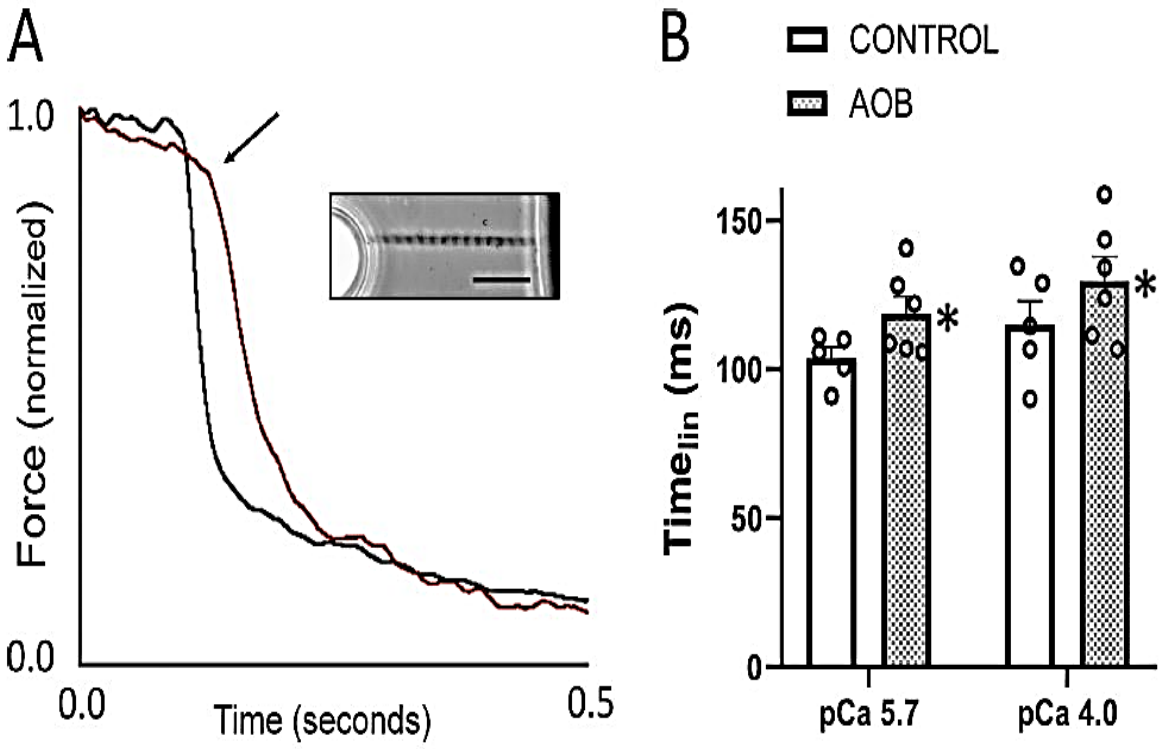

Figure 10. Single myofibril linear relaxation time. (A) Single myofibrils were attached to two glass probes, one of which was bent at a 90° angle to form a cantilever that allows for measurement of force (cf. A inset, 10 μM calibration bar; SL = 2.2 μm).Myofibrils were activated with either a maximum (pCa = 4.0) or ~50%maximum (pCa = 5.7) Ca2+-containing solutions using the rapid solution switching technique. Upon the rapid switch back to the low [Ca2+] solution (pCa = 9.0) at time = 0 s, myofibril force relaxed in a bi-phasic manner as illustrated in A. The time of transition from the slow to the fast relaxation phase (Timelin) in the AOB example trace is indicated by the arrow. (B) Average time of transition from the slow to the fast relaxation phase (Timelin) in Sham control (open bars) and AOB (closed bars) from either pCa = 4.0 or pCa = 5.7. n = 5 hearts per group. 15°C. Up to 30 myofibrils were studied per cohort. Subsequently, multiple muscle data were averaged to derive a single average datum per heart. *P = 0.041 Sham vs. AOB; P = 0.116 pCa = 4.0 vs. pCa = 5.7 by two-way ANOVA. Additional single myofibril data is presented in Fig. 9.

Single myofibril relaxation properties

Dynamic Ca2+ activation–relaxation dynamics were assessed by using the single myofibril technique (Poggesi et al., 2005; Stehle et al., 2009; Vitale et al., 2021). There were no differences in Ca2+ activation parameters between the Sham and AOB groups (results presented in Fig. 9). In contrast, the Ca2+ relaxation dynamics were significantly blunted in the AOB group, as illustrated in Fig. 10. Here, Fig. 10 A shows a typical force record obtained from a Sham and AOB single isolated LV myofibril (c.f. inset) upon a rapid switch from the activating to the relaxing solution (occurring at time = 0 s; note that force is normalized to the steady state maximum force development). As has been well described, myofilament relaxation upon the rapid withdrawal of activating Ca2+ is biphasic, where a slow relaxation phase transitions into a rapid phase of relaxation (Poggesi et al., 2005; Stehle et al., 2009; Vitale et al., 2021). The linear phase of relaxation which occurs prior to the onset

of the exponential decay of force (as indicated by the arrow in the figure) was significantly prolonged in the AOB group compared with the sham group. This delay in relaxation was apparent at submaximal and saturating calcium levels (Fig. 10). This is important as it corroborates slower cross-bridge cycling kinetics observed in skinned multicellular myocardium. Moreover, it also indicates that relaxation times are prolonged at activating Ca2+ levels likely to be operating in the working heart.

Discussion

In the present study, we adopted a guinea pig small rodent AOB model to study the role of myofilament function in the development of DHF. Guinea pigs were chosen as a model to avoid the impact of alterations in MHC isoform composition known to occur under stress in other small rodents (van der Velden and Stienen, 2019). We confirmed the absence of a significant MHC isoform shift. Actomyosin ATPase activity is largely dependent on the MHC isoform; α-MHC is at least three times faster than β-MHC (de Tombe and ter Keurs, 2012). This issue has been addressed in previous studies by generating β-MHC transgenic mice, studying propylthiouracil (PTU)-treated or thyroidectomized rats, and transgenic rabbits (Peterson and Alpert, 1996; Krenz et al., 2003; Rundell et al., 2005; Sadayappan et al., 2009; Suzuki et al., 2009). However, many of these methods can themselves transform the myofilament microenvironment such that results may not be directly applicable to humans, especially when studying pathological conditions.

AOB in guinea pigs resulted in congestive HF with signs of impaired ventricular relaxation without alterations in systolic function, consistent with DHF (HFpEF; Pfeffer et al., 2019). We characterized the end-stage DHF phenotype in our guinea pig model by recording cardiac morphometric ratios, echocardiography, and tissue Doppler measurements. Ejection fraction, a reduction of which is one of the most used clinical measures of heart failure, is in fact mostly preserved in cases of diastolic dysfunction (Maeder and Kaye, 2009). Pulse wave Doppler and tissue Doppler measurements are more sensitive toward detecting functional changes in the heart (Ommen et al., 2000; Zile and Brutsaert, 2002; Ho and Solomon, 2006). The mitral flow velocity profile recorded in the current AOB model corresponds to HF with pronounced diastolic dysfunction, characteristic of restrictive cardiomyopathy. To evaluate the underlying nature of diastolic dysfunction, we assessed the degree of fibrosis in this model (Edwards and O'Brien, 1980). Collagen deposition, although somewhat increased in the AOB model, was still minimal relative to that seen in a comparable rat or mouse model. Extracellular matrix remodeling is integral to HF progression in humans. The mild fibrotic response in guinea pig DHF is of particular importance as it implicates sarcomeric mechanisms and proteins being responsible for impaired relaxation in our model and not extracellular matrix remodeling. Moreover, the diastolic abnormality was also not caused by increased passive myofilament stiffness. Instead, various biophysical measurements indicated a reduction in the rate of cardiac cross-bridge detachment. Reduced cross-bridge cycling kinetics may be an important contributor to the development of DHF in larger mammals, including humans.

HF is an entity of increasing clinical significance (Tsao et al., 2022). About half of the patients suffer from HFpEF, with a bias toward the elderly female population (Maeder and Kaye, 2009; Pfeffer et al., 2019). This syndrome is caused by cardiac relaxation abnormalities

for which underlying cellular mechanisms are poorly understood. Moreover, treatment options to combat this syndrome have generally proven limited (Pfeffer et al., 2019). A disturbed cardiac myocyte Ca2+ homeostasis, in particular, a blunted rate of Ca2+ removal from the cytosol early in relaxation has been identified as a significant player in the development of diastolic pathology (Gilbert et al., 2020). However, based on studies employing either animal models or human samples, it has become evident that depressed myofilament function also contributes to the depressed cardiac function seen in both systolic and diastolic heart failure (de Tombe, 1998; Hamdani et al., 2008; van der Velden and de Tombe, 2014; van der Velden and Stienen, 2019).

It should be noted that while the present study focused on female guinea pigs, it has been reported that AOB in male guinea pigs also results in cardiac hypertrophy and heart failure (Siri et al., 1989), a finding we confirmed in preliminary studies leading up to the current study. We did find, however, that male guinea pigs are more fragile (i.e., premature deaths and other clinical complications) than female animals in response to cardiac stress, prompting us to focus on female subjects as reported in the current study.

The initial factors leading to cardiac and associated myofilament dysfunction may be acquired, for example, pressure or volume cardiac overload or chronic myocardial ischemia (de Tombe, 1998; Hamdani et al., 2008; van der Velden and de Tombe, 2014; van der Velden and Stienen, 2019). More recently, it has also become evident that inherited factors, such as mutations in cardiac myofilament proteins, may be causal to myofilament dysfunction that, in turn, and only in some patients, lead to cardiac dysfunction and failure (van der Velden and Stienen, 2019).

We and others have shown, in both animal models and human samples, a marked reduction in maximum myofilament force generating capacity (Fan et al., 1997; Belin et al., 2007; Daniels et al., 2007; Marston and de Tombe, 2008; van der Velden and de Tombe, 2014; Chung et al., 2019; van der Velden and Stienen, 2019). The current results obtained from isolated skinned myocyte fragments, but not multicellular and only trending in single myofibril preparations, are consistent with those previous findings. However, while a reduction in Fmax would be expected to play a significant role in depressed function in systolic heart failure, this is less clear in the DHF syndrome we observed in the present study. We did not, however, find any alteration in myofilament Ca2+ sensitivity upon pressure overload hypertrophy in the current study employing guinea pigs. There is a wide range of published results regarding this parameter, where either an increase, a decrease, or any change in Ca2+ sensitivity has been reported. The underlying cause(s) for the lack of consensus on this issue is not clear but could be related to contractile protein posttranslational modifications that may be poorly controlled, especially in the studies involving human samples (Marston and de Tombe, 2008). These data would suggest that the preserved pump function in our model results from compensated hypertrophic growth of the heart to overcome the underlying inability of sarcomeres to maintain tension in DHF.

In the current study, we found clear evidence for reduced cross-bridge cycling kinetics in response to pressure overload. That is, we found reduced force-dependent ATP consumption rate (tension-cost), reduced force redevelopment rate (Ktr), and prolongation of myofilament relaxation time (Timelin). We and others have previously reported similar findings in rat models of cardiac disease (Daniels et al., 2007; Zobel et al., 2007; Patel et al., 2017). However, as discussed above, a significant shift in myosin isoform expression is seen in this species during cardiac stress (Daniels et al., 2007). This phenomenon greatly limits the

translation of this finding to the human where such large isoform shifts do not occur, given the three-to-five times difference in kinetics between α- and β-MHC (Rundell et al., 2005). Few studies have addressed cross-bridge cycling kinetics in predominantly β-MHC myocardium in cardiac disease. In the guinea pig pressure overload model, Lecarpentier et al. (1987) have reported a reduced relaxation rate in twitching isolated cardiac papillary muscles, while Malhotra et al. (1992) reported a reduction in actomyosin ATPase rate in the same animal model. Finally, a reduction in cross-bridge kinetics has been reported in isolated failing human myocardium measured during steady state contractions (Ruf et al., 1998; Chung et al., 2019) or during Ca2+ activation following chemical permeabilization (Hajjar and Gwathmey, 1992; Vikhorev et al., 2022). Of interest, a recent study (Vitale et al., 2021) demonstrates that relaxation parameters derived from single myofibril experiments correlate with the measurement of tension-cost from the same isolated human samples, albeit with the caveat that sarcomeric mutations were studied that are associated with enhanced cross-bridge cycling kinetics. Nevertheless, this result validates the notion that both tension-cost and single myofibril relaxation parameters index cross-bridge cycling kinetics.

The underlying cellular and molecular mechanisms that lead to reduced cross-bridge cycling kinetics and force development are not clear. Previous studies in the pressure overload guinea pig model have not shown consistent alterations in contractile protein isoform composition or posttranslational modifications (Wang et al., 1999a; Foster et al., 2016). Likewise, in our current study, we failed to identify significant changes in the contractile proteome using 2-D–DIGE analysis, apart from a slight, but nonsignificant, reduction in troponin-I phosphorylation. Foster et al. (2016) did report significant alterations in metabolism-related pathways in the pressure overload guinea pig heart. Such changes could result in blunted ATP production leading to an “energy-starved heart” condition (Neubauer, 2007), which may reduce cross-bridge cycle kinetics and blunted cardiac power (Beard et al., 2022). However, such a mechanism cannot explain our current results that were obtained from chemically permeabilized tissue samples that were adequately supplied by a constant concentration of Mg-ATP. Future studies will be needed to elucidate the mechanisms underlying depressed cross-bridge cycling in DHF.

The use of animal models for the study of HF has been extensively reviewed (Hasenfuss, 1998; Riehle and Bauersachs, 2019; Pilz et al., 2022). Small animals, such as rats and mice, have been employed extensively but may be of limited value for human translation (Pilz et al., 2022). This limitation, due, in part to the high heart rate and predominant α-MHC expression in both rats and mice may be overcome by the deployment of large animal models (Pilz et al., 2022).

Limitations

In the current study, myofilament function was assessed at three different levels of integration: isolated myocyte fragments, isolated multicellular preparations, and isolated single myofibrils. Maximum force development was significantly blunted in isolated myocyte fragments, while this was not found in multicellular preparations or only trending in single myofibrils. It is likely that this is related to the procedure of normalization to cross-sectional area. This measurement is relatively robust in isolated myocyte fragments (Fan et al., 1997; Belin et al., 2007; Ait-Mou et al., 2016), but less so in the multicellular trabecula-like preparations that are obtained from frozen tissue by a low rpm grinding procedure (Witayavanitkul et al., 2014). The latter procedure leaves a layer of debris on the surface of the preparation that renders measurement of the cross-sectional area more difficult. Likewise,

the measurement of micrometer dimensions of single myofibrils using phase-contrast microscopy is fraught with uncertainty. Note that tension-cost is only impacted by muscle length, a parameter that can accurately be assessed, while Ktr does not depend on the dimensions of an individual muscle preparation.

Investigations such as the current study are invariably conducted using appropriate levels of anesthesia. As a result, the impact of anesthesia on either in vivo cardiac performance or ex vivo isolated muscle myofilament properties cannot be avoided and should be considered in interpreting our findings. We performed experiments using various sized preparations, ranging from the multicellular trabeculae-like preparation to myocyte fragments and single myofibrils. Each of these was assessed at different temperatures. That is, ATPase experiments were performed at 25°C to ensure sufficient ATPase activity, while single myofibril experiments were performed at 15°C to reduce rundown. Therefore, a possible confounding impact of temperature (de Tombe and Stienen, 2007) needs to be taken into account when interpreting our results.

The absolute composition of the skinned fiber solutions is fraught with uncertainty, particularly as it relates to the free [Ca2+] and [Mg2+]. This is due to uncertainties pertaining to many of the chemical binding constants (and their temperature dependencies) that are required to calculate/estimate solution compositions. Note that the ATPase solutions are based on a phosphoenolpyruvate/pyruvate kinase ATP regeneration system, while the myocyte fragment solutions are based on a creatine phosphate/ creatine kinase ATP regeneration system. Therefore, it should be noted that calcium sensitivity parameters (EC50) cannot be compared across these varying solution modalities.

While reduced cross-bridge cycling was found in the ATPase tension-cost experiments on multicellular preparation, this was less pronounced in the single myofibril experiments where only a prolongation of the linear phase of relaxation was observed. The reasons underlying this discrepancy are not entirely clear but may be related to the large temperature difference (25 vs. 15°C) between these experimental modalities.

Conclusions

We developed a clinically relevant β-myosin (guinea pig) model of heart failure with preserved ejection fraction. To the best of our knowledge, this is the first study to describe the alterations in actomyosin cross-bridge cycling kinetics in a β-MHC model of DHF. Also, this study is among the first to index a hypertensive model of DHF in the female population in an animal closely mimicking the human DHF phenotype. We conclude that impaired cross-bridge cycle kinetics contribute, at least in part, to the diastolic cardiac pathology that is seen in this model.

Data availability

Source data will be made freely available upon request if addressed to the corresponding author.

Acknowledgments

Henk L. Granzier served as editor.

We would like to thank Shamim Chowdhury, David Geenen, Milana Grachoff, Kirsten Kulek, and Kelly Schoenefelt for assistance with this study.

This study was supported, in part, by National Institutes of Health grant P01-HL062426.

Author contributions:

S. Dewan, N. Witayavanitkul, M. Kumar, and B. Mayer performed experiments; S. Dewan and P. de Tombe designed experiments and supervised the research; S. Dewan, O. Cazorla, L. Betancourt, and P. de Tombe analyzed data and edited the manuscript.

Disclosures:

The authors declare no competing interests exist.

References

Ait-Mou, Y., K. Hsu, G.P. Farman, M. Kumar, M.L. Greaser, T.C. Irving, and P.P. de Tombe. 2016. Titin strain contributes to the Frank-Starling law of the heart by structural rearrangements of both thin- and thickfilament proteins. Proc. Natl. Acad. Sci. USA. 113:2306–2311. https://doi.org/10.1073/pnas.1516732113

Beard, D.A., B. Marzban, O.Y. Li, K.S. Campbell, P.M.L. Janssen, N.C. Chesler, and A.J. Baker. 2022. Reduced cardiac muscle power with low ATP simulating heart failure. Biophys. J. 121:3213–3223. https://doi.org/10.1016/j.bpj.2022.07.029

Belin, R.J., M.P. Sumandea, E.J. Allen, K. Schoenfelt, H. Wang, R.J. Solaro, and P.P. de Tombe. 2007. Augmented protein kinase C-α–induced myofilament protein phosphorylation contributes to myofilament dysfunction in experimental congestive heart failure. Circ. Res. 101:195–204. https://doi.org/10.1161/CIRCRESAHA.107.148288

Bers, D.M. 2002. Cardiac excitation-contraction coupling. Nature. 415:198–205. https://doi.org/10.1038/415198a

Brenner, B. 1991. Rapid dissociation and reassociation of actomyosin crossbridges during force generation: A newly observed facet of cross-bridge action in muscle. Proc. Natl. Acad. Sci. USA. 88:10490–10494. https://doi.org/10.1073/pnas.88.23.10490

Chen, Y., A. Somji, X. Yu, and J.E. Stelzer. 2010. Altered in vivo left ventricular torsion and principal strains in hypothyroid rats.Am. J. Physiol. HeartCirc. Physiol. 299:H1577–H1587. https://doi.org/10.1152/ajpheart.00406.2010

Chung, J.H., N. Milani-Nejad, J.P. Davis, N. Weisleder, B.A. Whitson, P.J. Mohler, and P.M.L. Janssen. 2019. Impact of heart rate on cross-bridge cycling kinetics in failing and nonfailing human myocardium. Am. J. Physiol. Heart Circ. Physiol. 317:H640–H647. https://doi.org/10.1152/ajpheart.00163.2019

Daniels,M.C., T. Naya, V.L. Rundell, and P.P. de Tombe. 2007. Development of contractile dysfunction in rat heart failure: Hierarchy of cellular events. Am. J. Physiol. Regul. Integr. Comp. Physiol. 293:R284–R292. https://doi.org/10.1152/ajpregu.00880.2006

de Tombe, P.P. 1998. Altered contractile function in heart failure. Cardiovasc. Res. 37:367–380. https://doi.org/10.1016/S0008-6363(97)00275-7

de Tombe, P.P. 2003. Cardiac myofilaments: Mechanics and regulation. J. Biomech. 36:721–730. https://doi.org/10.1016/S0021-9290(02)00450-5

de Tombe, P.P., and G.J. Stienen. 2007. Impact of temperature on cross-bridge cycling kinetics in rat myocardium. J. Physiol. 584:591–600. https://doi.org/10.1113/jphysiol.2007.138693

de Tombe, P.P., and H.E. ter Keurs. 2012. The velocity of cardiac sarcomere shortening: Mechanisms and implications. J. Muscle Res. Cell Motil. 33: 431–437. https://doi.org/10.1007/s10974-012-9310-0

Edwards, C.A., and W.D. O'Brien Jr. 1980. Modified assay for determination of hydroxyproline in a tissue hydrolyzate. Clin. Chim. Acta. 104:161–167. https://doi.org/10.1016/0009-8981(80)90192-8

Fan, D., T.Wannenburg, and P.P. de Tombe. 1997. Decreased myocyte tension development and calcium responsiveness in rat right ventricular pressure overload. Circulation. 95:2312–2317. https://doi.org/10.1161/01.CIR.95.9.2312

Foster, D.B., T. Liu, K. Kammers, R. O'Meally, N. Yang, K.N. Papanicolaou, C.C. Talbot Jr, R.N. Cole, and B. O'Rourke. 2016. Integrated omic analysis of a Guinea pig model of heart failure and sudden cardiac death. J. Proteome Res. 15:3009–3028. https://doi.org/10.1021/acs.jproteome.6b00149

Gilbert, G., K. Demydenko, E. Dries, R.D. Puertas, X. Jin, K. Sipido, and H.L. Roderick. 2020. Calciumsignaling in cardiomyocyte function. Cold Spring Harb. Perspect. Biol. 12:12. https://doi.org/10.1101/cshperspect.a035428

Gordon, A.M., E. Homsher, and M. Regnier. 2000. Regulation of contraction in striated muscle. Physiol. Rev. 80:853–924. https://doi.org/10.1152/physrev.2000.80.2.853

Hajjar, R.J., and J.K. Gwathmey. 1992. Cross-bridge dynamics in human ventricular myocardium. Regulation of contractility in the failing heart. Circulation. 86:1819–1826. https://doi.org/10.1161/01.CIR.86.6.1819

Hamdani, N., V. Kooij, S. van Dijk, D. Merkus, W.J. Paulus, C.D. Remedios, D.J. Duncker, G.J. Stienen, and J. van der Velden. 2008. Sarcomeric dysfunction in heart failure. Cardiovasc. Res. 77:649–658. https://doi.org/10.1093/cvr/cvm079

Hasenfuss, G. 1998. Animal models of human cardiovascular disease, heart failure and hypertrophy. Cardiovasc. Res. 39:60–76. https://doi.org/10.1016/S0008-6363(98)00110-2

Henein, M.Y., and P. Lindqvist. 2020. Diastolic function assessment by echocardiography: A practical manual for clinical use and future applications. Echocardiography. 37:1908–1918. https://doi.org/10.1111/echo.14698

Ho, C.Y., and S.D. Solomon. 2006. A clinician's guide to tissue Doppler imaging. Circulation. 113:e396–e398. https://doi.org/10.1161/CIRCULATIONAHA.105.579268

Johns, E.C., K.O. Ryder, E.A. Hodson, G. Hart, I.P. Mulligan, S. Lipscomb, and C.C. Ashley. 1999. Investigating the relaxation rate, following diazo- 2 photolysis, of a skinned trabecular preparation from guinea-pig hypertrophied eft ventricle. Pflugers Arch. 438:771–777. https://doi.org/10.1007/s004249900131

Krenz, M., A. Sanbe, F. Bouyer-Dalloz, J. Gulick, R. Klevitsky, T.E. Hewett, H.E. Osinska, J.N. Lorenz, C. Brosseau, A. Federico, et al. 2003. Analysis of myosin heavy chain functionality in the heart. J. Biol. Chem. 278: 17466–17474. https://doi.org/10.1074/jbc.M210804200

Lecarpentier, Y., A. Waldenstr¨om, M. Clergue, D. Chemla, P. Oliviero, J.L. Martin, and B. Swynghedauw. 1987. Major alterations in relaxation during cardiac hypertrophy induced by aortic stenosis in guinea pig. Circ. Res. 61:107–116. https://doi.org/10.1161/01.RES.61.1.107

Locher, M.R., M.V. Razumova, J.E. Stelzer, H.S. Norman, and R.L. Moss. 2011. Effects of low-level α-myosin heavy chain expression on contractile kinetics in porcine myocardium. Am. J. Physiol. Heart Circ. Physiol. 300: H869–H878. https://doi.org/10.1152/ajpheart.00452.2010

Locher, M.R., M.V. Razumova, J.E. Stelzer, H.S. Norman, J.R. Patel, and R.L. Moss. 2009. Determination of rate constants for turnover of myosin isoforms in rat myocardium: Implications for in vivo contractile kinetics. Am. J. Physiol. Heart Circ. Physiol. 297:H247–H256. https://doi.org/10.1152/ajpheart.00922.2008

Maeder, M.T., and D.M. Kaye. 2009. Heart failure with normal left ventricular ejection fraction. J. Am. Coll. Cardiol. 53:905–918. https://doi.org/10.1016/j.jacc.2008.12.007

Malhotra, A., F.M. Siri, and R. Aronson. 1992. Cardiac contractile proteins in hypertrophied and failing Guinea pig heart. Cardiovasc. Res. 26:153–161. https://doi.org/10.1093/cvr/26.2.153

Marston, S.B., and P.P. de Tombe. 2008. Troponin phosphorylation and myofilament Ca2+-sensitivity in heart failure: Increased or decreased?. J. Mol. Cell. Cardiol. 45:603–607. https://doi.org/10.1016/j.yjmcc.2008.07.004

Miyata, S., W. Minobe, M.R. Bristow, and L.A. Leinwand. 2000. Myosin heavy chain isoform expression in the failing and nonfailing human heart. Circ. Res. 86:386–390. https://doi.org/10.1161/01.RES.86.4.386

Neubauer, S. 2007. The failing heart—an engine out of fuel. N. Engl. J. Med. 356:1140–1151. https://doi.org/10.1056/NEJMra063052

Ommen, S.R., R.A. Nishimura, C.P. Appleton, F.A. Miller, J.K. Oh, M.M. Redfield, and A.J. Tajik. 2000. Clinical utility of Doppler echocardiography and tissue Doppler imaging in the estimation of left ventricular filling pressures: A comparative simultaneous Doppler-catheterization study. Circulation. 102:1788–1794. https://doi.org/10.1161/01.CIR.102.15.1788

Patel, J.R., G.P. Barton, R.K. Braun, K.N. Goss, K. Haraldsdottir, A. Hopp, G. Diffee, T.A. Hacker, R.L. Moss, and M.W. Eldridge. 2017. Altered right ventricular mechanical properties are afterload dependent in a rodent model of bronchopulmonary dysplasia. Front. Physiol. 8:840. https://doi.org/10.3389/fphys.2017.00840

Peterson, J.N., and N.R. Alpert. 1996. Molecular motor mechanics in the contracting heart. V1 versus V3 myosin heavy chain. Ann. N. Y. Acad. Sci. 793:54–63. https://doi.org/10.1111/j.1749-6632.1996.tb33504.x

Pfeffer, M.A., A.M. Shah, and B.A. Borlaug. 2019. Heart failurewith preserved ejection fraction in perspective. Circ. Res. 124:1598–1617. https://doi.org/10.1161/CIRCRESAHA.119.313572

Pilz, P.M., J.E. Ward, W.T. Chang, A. Kiss, E. Bateh, A. Jha, S. Fisch, B.K. Podesser, and R. Liao. 2022. Large and small animal models of heart failure with reduced ejection fraction. Circ. Res. 130:1888–1905. https://doi.org/10.1161/CIRCRESAHA.122.320246

Poggesi, C., C. Tesi, and R. Stehle. 2005. Sarcomeric determinants of striated muscle relaxation kinetics. Pflugers Arch. 449:505–517. https://doi.org/10.1007/s00424-004-1363-5

Riehle, C., and J. Bauersachs. 2019. Small animal models of heart failure. Cardiovasc. Res. 115:1838–1849. https://doi.org/10.1093/cvr/cvz161

Ruf, T., H. Schulte-Baukloh, J. Lüdemann, H. Posival, F. Beyersdorf, H. Just, and C. Holubarsch. 1998. Alterations of cross-bridge kinetics in human atrial and ventricular myocardium. Cardiovasc. Res. 40:580–590. https://doi.org/10.1016/S0008-6363(98)00164-3

Rundell, V.L., D.L. Geenen, P.M. Buttrick, and P.P. de Tombe. 2004. Depressed cardiac tension cost in experimental diabetes is due to altered myosin heavy chain isoform expression. Am. J. Physiol. Heart Circ. Physiol. 287:H408–H413. https://doi.org/10.1152/ajpheart.00049.2004

Rundell, V.L., V. Manaves, A.F. Martin, and P.P. de Tombe. 2005. Impact of β-myosin heavy chain isoform expression on cross-bridge cycling kinetics. Am. J. Physiol. Heart Circ. Physiol. 288:H896–H903. https://doi.org/10.1152/ajpheart.00407.2004

Sadayappan, S., J. Gulick, R. Klevitsky, J.N. Lorenz, M. Sargent, J.D. Molkentin, and J. Robbins. 2009. Cardiac myosin binding protein-C phosphorylation in a β-myosin heavy chain background. Circulation. 119: 1253–1262. https://doi.org/10.1161/CIRCULATIONAHA.108.798983

Siri, F.M., C. Nordin, S.M. Factor, E. Sonnenblick, and R. Aronson. 1989. Compensatory hypertrophy and failure in gradual pressure-overloaded guinea pig heart. Am. J. Physiol. 257:H1016–H1024. https://doi.org/10.1152/ajpheart.1989.257.3.H1016

Stegemann, H., and K. Stalder. 1967. Determination of hydroxyproline. Clin. Chim. Acta. 18:267–273. https://doi.org/10.1016/0009-8981(67)90167-2

Stehle, R., J. Solzin, B. Iorga, and C. Poggesi. 2009. Insights into the kinetics of Ca2+-regulated contraction and relaxation from myofibril studies. Pflugers Arch. 458:337–357. https://doi.org/10.1007/s00424-008-0630-2

Suzuki, T., B.M. Palmer, J. James, Y. Wang, Z. Chen, P. VanBuren, D.W. Maughan, J. Robbins, and M.M. LeWinter. 2009. Effects of cardiac myosin isoform variation on myofilament function and crossbridge kinetics in transgenic rabbits. Circ. Heart Fail. 2:334–341. https://doi.org/10.1161/CIRCHEARTFAILURE.108.802298

Tsao, C.W., A.W. Aday, Z.I. Almarzooq, A. Alonso, A.Z. Beaton, M.S. Bittencourt, A.K. Boehme, A.E. Buxton, A.P. Carson, Y. Commodore-Mensah, et al. 2022. Heart disease and stroke statistics-2022 update: A report from the American Heart Association. Circulation. 145:e153–e639.https://doi.org/10.1161/CIR.0000000000001052

van der Velden, J. 2011. Diastolic myofilament dysfunction in the failing human heart. Pflugers Arch. 462:155–163. https://doi.org/10.1007/s00424-011-0960-3

van der Velden, J., and P.P. de Tombe. 2014. Heart failure: A special issue. Pflugers Arch. 466:1023. https://doi.org/10.1007/s00424-014-1531-1

van der Velden, J., A.F. Moorman, and G.J. Stienen. 1998. Age-dependent changes in myosin composition correlate with enhanced economy of contraction in guinea-pig hearts. J. Physiol. 507:497–510. https://doi.org/10.1111/j.1469-7793.1998.497bt.x

van der Velden, J., and G.J.M. Stienen. 2019. Cardiac disorders and pathophysiology of sarcomeric proteins. Physiol. Rev. 99:381–426. https://doi .org/10.1152/physrev.00040.2017

Vikhorev, P.G., N.N. Vikhoreva, W. Yeung, A. Li, S. Lal, C.G. Dos Remedios, C.A. Blair, M. Guglin, K.S. Campbell, M.H. Yacoub, et al. 2022. Titin- truncating mutations associated with dilated cardiomyopathy alter length-dependent activation and its modulation via phosphorylation. Cardiovasc. Res. 118:241–253. https://doi.org/10.1093/cvr/cvaa316

Vitale, G., C. Ferrantini, N. Piroddi, B. Scellini, J.M. Pioner, B. Colombini, C. Tesi, and C. Poggesi. 2021. The relation between sarcomere energetics and the rate of isometric tension relaxation in healthy and diseased cardiac muscle. J. Muscle Res. Cell Motil. 42:47–57. https://doi.org/10.1007/s10974-019-09566-2

Wang, X., F. Li, S.E. Campbell, and A.M. Gerdes. 1999a. Chronic pressure overload cardiac hypertrophy and failure in Guinea pigs: II. Cytoskeletal remodeling. J. Mol. Cell. Cardiol. 31:319–331. https://doi.org/10.1006/jmcc.1998.0885

Wang, X., F. Li, and A.M. Gerdes. 1999b. Chronic pressure overload cardiac hypertrophy and failure in Guinea pigs: I. Regional hemodynamics and myocyte remodeling. J. Mol. Cell. Cardiol. 31:307–317. https://doi.org/10.1006/jmcc.1998.0884

Warren, C.M., G.M. Arteaga, S. Rajan, R.P. Ahmed, D.F. Wieczorek, and R.J. Solaro. 2008. Use of 2-D DIGE analysis reveals altered phosphorylation in a tropomyosin mutant (Glu54Lys) linked to dilated cardiomyopathy. Proteomics. 8:100–105. https://doi.org/10.1002/pmic.200700772

Witayavanitkul, N., Y. Ait Mou, D.W. Kuster, R.J. Khairallah, J. Sarkey, S. Govindan, X. Chen, Y. Ge, S. Rajan, D.F. Wieczorek, et al. 2014. Myocardial infarction-induced N-terminal fragment of cardiac myosinbinding protein C (cMyBP-C) impairs myofilament function in human myocardium. J. Biol. Chem. 289:8818–8827. https://doi.org/10.1074/jbc.M113.541128

Zile, M.R., and D.L. Brutsaert. 2002. New concepts in diastolic dysfunction and diastolic heart failure: Part I: Diagnosis, prognosis, and measurements of diastolic function. Circulation. 105:1387–1393. https://doi.org/ 10.1161/hc1102.105289

Zobel, C., P. Zavidou-Saroti, B. B¨olck, K. Brixius, H. Reuter, K. Frank, H. Diedrichs, J. Müller-Ehmsen, W. Bloch, and R.H. Schwinger. 2007. Altered tension cost in (TG(mREN-2)27) rats overexpressing the mouse renin gene. Eur. J. Appl. Physiol. 99:121–132. https://doi.org/10.1007/s00421-006-0323-5